ADVANCED ELECTRONIC MATERIALS
www.advelectronicmat.de

Negative Isotope Effect on Field-Effect Hole Transport in Fully Substituted ^{13}C-Rubrene

*Xinglong Ren, Matthew J. Bruzek, David A. Hanifi, Aaron Schulzetenberg, Yanfei Wu, Chang-Hyun Kim, Zhuoran Zhang, James E. Johns, Alberto Salleo, Simone Fratini, Alessandro Troisi, Christopher J. Douglas, and C. Daniel Frisbie**

Isotopic substitution is a useful method to study the influence of nuclear motion on the kinetics of charge transport in semiconductors. However, in organic semiconductors, no observable isotope effect on field-effect mobility has been reported. To understand the charge transport mechanism in rubrene, the benchmark organic semiconductor, crystals of fully isotopically substituted rubrene, ^{13}C-rubrene ($^{13}C_{42}H_{28}$), are synthesized and characterized. Vapor-grown ^{13}C-rubrene single crystals have the same crystal structure and quality as native rubrene crystals (i.e., rubrene with a natural abundance of carbon isotopes). The characteristic transport signatures of rubrene, including room temperature hole mobility over 10 cm^2 V^{-1} s^{-1}, intrinsic band-like transport, and clear Hall behavior in the accumulation layer of air-gap transistors, are also observed for ^{13}C-rubrene crystals. The field-effect mobility distributions based on 74 rubrene and ^{13}C-rubrene devices, respectively, reveal that ^{13}C isotopic substitution produces a 13% reduction in the hole mobility of rubrene. The origin of the negative isotope effect is linked to the redshift of vibrational frequencies after ^{13}C-substitution, as demonstrated by computer simulations based on the transient localization (dynamic disorder) scenario. Overall, the data and analysis provide an important benchmark for ongoing efforts to understand transport in ordered organic semiconductors.

The intrinsic transport properties of organic semiconductors are naturally best investigated in single crystals due to the generally low level of static disorder in these samples.[1–4] Field-effect transport measurements on crystals of the benchmark organic semiconductor rubrene ($C_{42}H_{28}$, 532.7 g mol^{-1}), in particular, have been pivotal for organic electronics as they have revealed the simultaneous presence of both high room temperature hole mobility above 10 cm^2 V^{-1} s^{-1}[5] and, crucially, a negative temperature exponent for the mobility, i.e., mobility increases as temperature decreases down to about 180 K.[6] These observations and others, including mobility anisotropy[7,8] and a robust Hall effect,[9,10] are strong evidence for band-like transport in rubrene (bandwidth ≈0.5 eV),[11] where many features of classical band transport are observed. However, the estimated carrier mean free paths remain on the order of the unit cell dimension (≈1 nm), thus precluding the typical band picture in conventional semiconductors.

The precise nature of band-like transport in organic semiconductor crystals is still being explored.[12] Currently, a consistent picture of charge transport in high mobility crystals is offered by the dynamic disorder model (DDM, also known as transient localization), in which the carrier transient localization length l_{loc} and the propagation rate ω are determined by a competition between intermolecular electronic coupling and charge–phonon interaction; in this scenario the carrier mobility μ can be evaluated as[13]

$$\mu = \frac{e}{k_B T} l_{loc}^2 \omega \quad (1)$$

X. Ren, Dr. Y. Wu, C.-H. Kim, Prof. C. D. Frisbie
Department of Chemical Engineering and Materials Science
University of Minnesota
Minneapolis, MN 55455, USA
E-mail: frisbie@umn.edu
Dr. M. J. Bruzek, A. Schulzetenberg, Z. Zhang, Prof. J. E. Johns, Prof. C. J. Douglas
Department of Chemistry
University of Minnesota
Minneapolis, MN 55455, USA
D. A. Hanifi
Department of Chemistry
Stanford University
Stanford, CA 94305, USA
Prof. A. Salleo
Department of Materials Science and Engineering
Stanford University
Stanford, CA 94305, USA
Dr. S. Fratini
Institut Néel-CNRS and Université Grenoble Alpes
F-38042 Grenoble, France
Prof. A. Troisi
Department of Chemistry and Centre for Scientific Computing
University of Warwick
Coventry CV4 7AL, UK

DOI: 10.1002/aelm.201700018

Here, ω^{-1} can be viewed as the characteristic time that charge is transiently localized due to the lattice dynamics, and it is set by the predominant low frequency intermolecular modes that modulate the intermolecular electronic coupling; l_{loc} is the length that charge can spread within the characteristic time ω^{-1}, and is limited by the dynamic disorder as well as the intermolecular transfer integral. l_{loc} decreases with temperature because higher temperatures lead to higher degrees of dynamic disorder, reducing intermolecular coupling. Indeed, the degree to which low frequency vibrations modify charge-transfer integrals was recently investigated by thermal diffuse electron diffraction scattering in crystalline 6,13-bis(triisopropylsilylethynyl)pentacene (TIPS-pentacene), combined with quantum chemical calculations, and it was shown that intermolecular coupling can change by over 100% relative to equilibrium values.[14]

The high hole mobility in orthorhombic crystalline rubrene is generally attributed to the large intermolecular transfer integrals (few tenths of eV) together with a relatively weak coupling of the charge carriers to the relevant intermolecular vibrations, both enhancing l_{loc} (≈5 nm at room temperature).[15–17] Further, the expectation from DDM is that increasing (decreasing) the frequency of lattice phonons will increase (decrease) the charge mobility because the charge remains localized for shorter (longer) periods of time, i.e., ideally $\mu \sim \omega$.[13] For rubrene, 100% substitution of the ^{13}C isotope into the molecular structure produces an ≈8% increase in molecular mass, which can be anticipated to produce an ≈4% decrease in intermolecular vibrational frequency and thus a comparable decrease in charge mobility. In contrast, a true band transport system dominated by acoustic phonon scattering has no isotope effect on mobility.[18,19] Thus, the study of isotopically labeled organic semiconductors with identical electronic structures but changed molecular masses offers the opportunity to confirm expectations of DDM. Furthermore, although isotopic substitution was introduced into organic electronics in the 1970s, largely in conjunction with time-of-flight mobility measurements, the conclusions of these earlier experiments were mixed, with reports of both positive and negative isotope effects for very similar systems.[20–26] Thus, the opportunity to clarify the nature of the kinetic isotopic effect in crystalline organic semiconductors provides an additional motivation. It is worth noting that Shuai and co-workers have suggested that nuclear tunneling may play a role in charge transport of carbon-based materials, and their hopping model also predicts a significant negative isotope effect on charge mobility upon ^{13}C-substitution.[19,27] Such a hopping model, which is based on a modified Marcus picture, is however only strictly valid in the narrow-band limit, which does not apply to rubrene.

Here we report our experimental and theoretical investigations of field-effect transport in ^{13}C-rubrene ($^{13}C_{42}H_{28}$, 574 g mol^{-1}) single crystals. We synthesized ^{13}C-rubrene, grew the single crystals from the vapor phase, and performed structural and electrical characterizations. The results confirm that the crystal structure of ^{13}C-rubrene is identical to native rubrene. We find a surprisingly significant negative isotope effect of −13% on the mobility, which is consistent with DDM, though the effect is somewhat larger than DDM simulations predict.[16] Importantly, our results also demonstrate definitively that semi-classical band transport is not the transport mechanism in rubrene. To the best of our knowledge, this is the first report of a negative isotope effect on field-effect charge transport in an organic semiconductor and the data provide an important benchmark for ongoing theoretical investigations of the properties of organic semiconductors.

The detailed synthetic route to ^{13}C-rubrene can be found in the Supporting Information. Single crystals were grown by the horizontal physical vapor transport method.[28] X-ray diffraction (XRD) and atomic force microscopy (AFM) were used to examine the quality of the crystals. **Figure 1**a displays the wide-angle diffraction patterns for ^{13}C-rubrene and native rubrene single crystals. All the diffraction peaks observed correspond to the family of (002) planes. In a direct comparison between the peaks from ^{13}C-rubrene and native rubrene single crystals, we can see that the positions of corresponding (*hkl*) peaks are almost identical, which implies that they share the same crystal structure and lattice constant. Moreover, AFM height images (Figure 1b) show that the surfaces of both rubrene and ^{13}C-rubrene crystals are clean and molecularly flat, with an average step height of 1.3 nm. The step height is close to the interlayer distance along the *c*-axis, which is 1.34 nm calculated from Bragg's Law for the (002) reflection. In addition, the crystals were analyzed by single-crystal X-ray crystallography (see the Supporting Information) and revealed a solid-state packing essentially identical to that of native rubrene.[29] The structural characterization was crucial to this study to ensure that no large difference in measured transistor properties could be attributed to differences in crystal structure. This confirms that those crystals with good crystallinity and clean, flat surfaces are qualified for the fabrication of single crystal field-effect transistors (FETs). Importantly, by Raman spectroscopy we observed a clear isotope effect on low-wavenumber intermolecular modes (Figure 1c). Peaks from the ^{13}C-rubrene sample in the range of 40–200 cm^{-1} appeared at systematically lower wavenumbers, as predicted. These low frequency modes are expected to be critical for transport as they transiently modulate the intermolecular transfer integrals. For example, the Raman peak at 48.0 cm^{-1} shifts to 46.3 cm^{-1} after ^{13}C-substitution, a 3.5% decrease, which is expected to cause a comparable decrease in mobility according to Equation (1). In addition, the high-wavenumber modes were also investigated by both IR and Raman (Supporting Information), demonstrating that ^{13}C-substitution leads to a redshift for all the vibrational modes in rubrene.

Air-gap transistors based on ^{13}C-rubrene single crystals were fabricated on PDMS substrates according to earlier publications.[5,7] The device structure is shown in **Figure 2**a. The ^{13}C-rubrene single crystal transistors exhibit p-type operation like native rubrene transistors, in which the semiconducting channel opens at negative gate bias ($V_g < 0$ V). The lack of hysteresis in both transfer curves (Figure 2b) and output curves (Figure 2c) is evidence for a low density of trap states at the rubrene/air interface, as can be expected for the air-gap structure.[30] As shown in Figure 2b, the device turns on near $V_g = 0$ V and has an on/off ratio of ≈10^4. For $V_d = -1$ V, −2 V, and −5 V, the device operates in the linear regime at large V_g, and the perfectly linear transfer curves are indicative of a high quality single crystal FET. The field-effect mobility can be calculated by the standard FET equation ($V_d \ll V_g - V_{th}$)

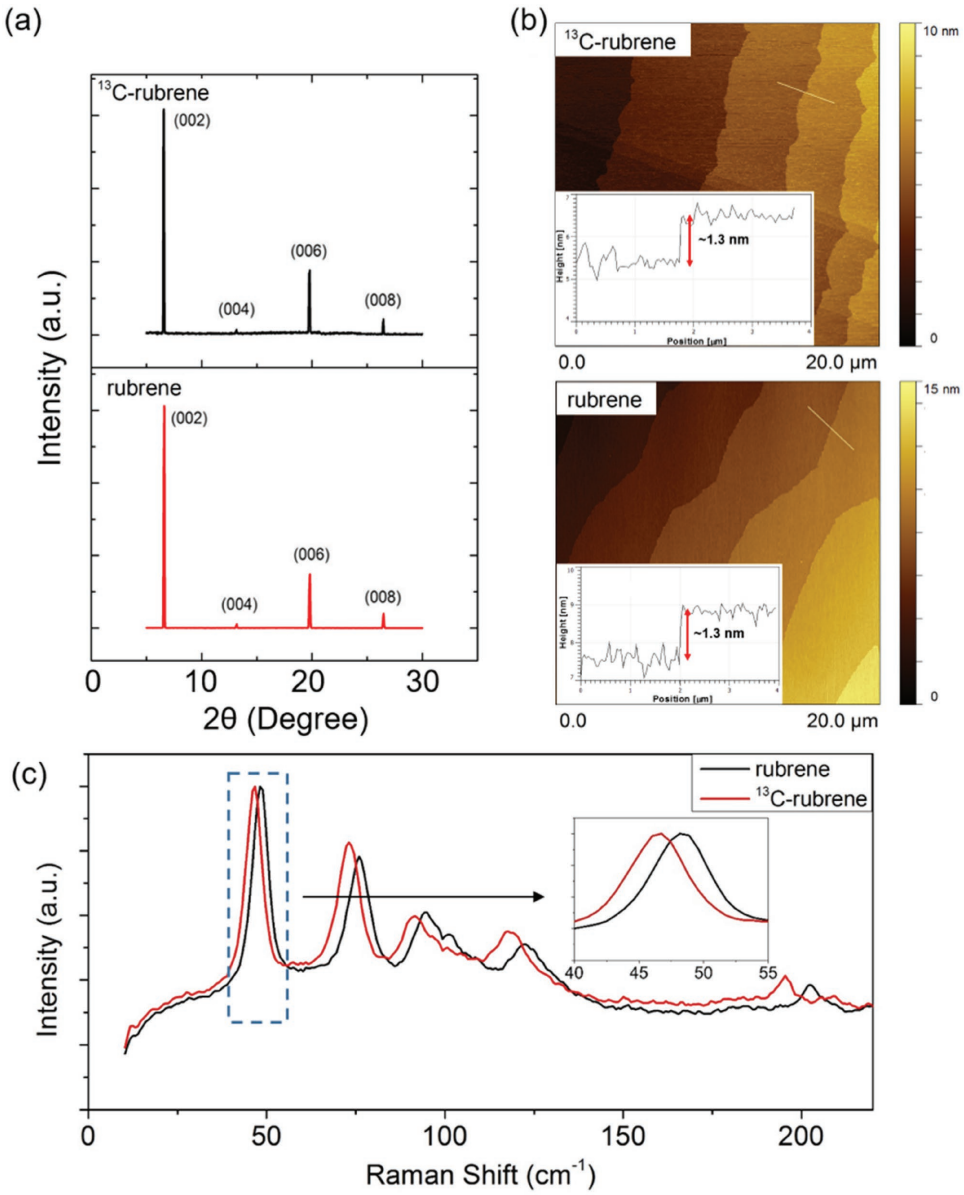

Figure 1. Structural characterization of rubrene and ^{13}C-rubrene. a) Wide-angle X-ray diffraction patterns. b) Tapping-mode atomic force microscopy height images (inset: height profiles of the white lines in the image). c) Low-wavenumber Raman spectrum (inset: zoomed-in image of the first peak). The crystal structures are identical, but all the vibrational modes are shifted to lower frequencies.

$$I_d = \frac{W}{L} C\mu V_d \left(V_g - V_{th}\right) \tag{2}$$

where W and L are the width and length of the semiconducting channel, C is the specific gate capacitance (for the 5 μm gap, $C \approx 0.18$ nF cm^{-2}), and V_{th} is the threshold voltage, which is determined by the intercept from linear extrapolation of I_d to the V_g axis. Regardless of the drain voltage, the device shown in Figure 2b has a threshold voltage of ≈ –5.5 V and a hole mobility of 15.3 cm^2 V^{-1} s^{-1}, which is a typical value for high-performance single crystal air-gap FETs. From the output characteristics in Figure 2c, a linear I_d–V_d relationship at low bias confirms the Ohmic nature of the metal/semiconductor contacts, implying that the hole injection barrier at the contacts is very low, which may originate from the alignment of the highest occupied molecular orbital (HOMO) level of ^{13}C-rubrene with the work function of Au.[31]

Variable-temperature electrical measurements were employed to elucidate the charge transport behavior of ^{13}C-rubrene single crystals, and were carried out on devices with a four-probe configuration to correct for temperature-dependent contact resistance.[32] Two voltage-sensing probes were inserted into the channel to measure the real potential drop within the channel. In this configuration, the contact-corrected four-probe field-effect mobility (μ_{4p}) is calculated by

$$\mu_{4p} = \frac{\Delta L}{WC} \frac{\partial \frac{I_d}{\Delta V}}{\partial V_g} \tag{3}$$

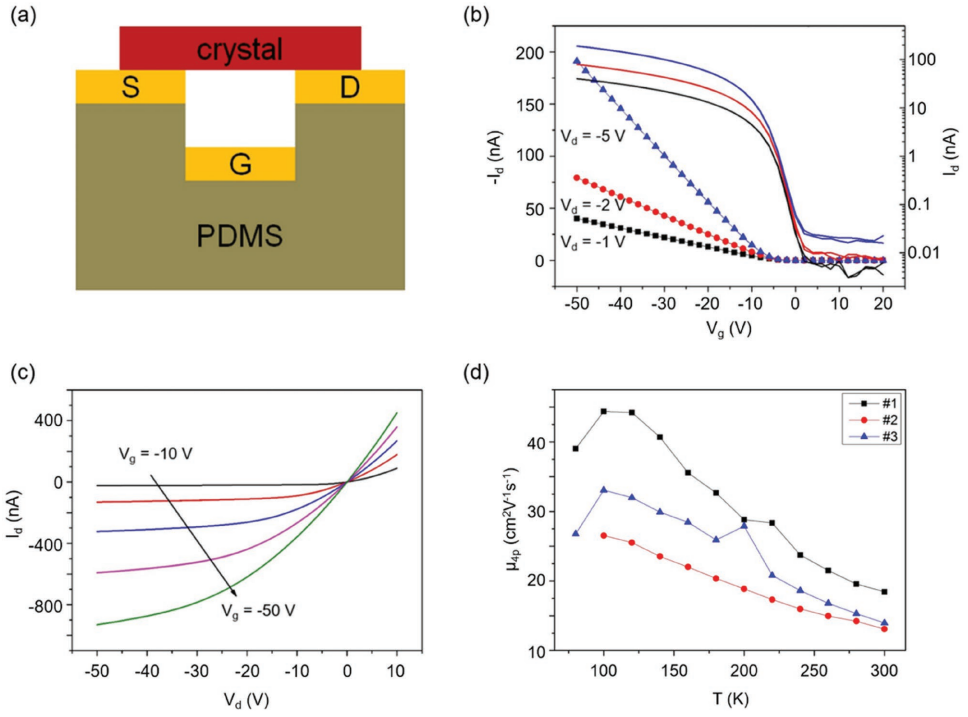

Figure 2. a) Cross section of the device structure. b) Room temperature transfer characteristics of a device in linear scale (left axis) and log scale (right axis). c) Room temperature output curves of the same device with gate voltages from −10 to −50 V. (Device dimensions: L = 300 µm, W = 100 µm.) d) Temperature dependence of the mobility for three different ^{13}C-rubrene devices. Band-like transport persists to 100 K in these samples. (Device dimensions: device #1: W = 130 µm, L = 150 µm, ΔL = 70 µm; device #2: W = 90 µm, L = 300 µm, ΔL = 180 µm; device #3: W = 80 µm, L = 300 µm, ΔL = 180 µm.)

where ΔL and ΔV are, respectively, the distance and the potential difference between the two reference probes. The μ_{4p} versus T relationships for three different devices are presented in Figure 2d. It is clear that the mobility increases with decreasing temperature ($d\mu/dT < 0$), which implies that band-like transport is operative in ^{13}C-rubrene single crystals. During the cooling process, some of the crystals broke apart, which is common for this device architecture due to the difference in thermal contraction for rubrene versus the PDMS stamp. For those crystals that did not crack, when they were heated back to 300 K, the mobility returned to the original value, indicating that the devices did not suffer any thermal degradation during the thermal cycle. The band-like transport phenomenon is reproducible in ^{13}C-rubrene single crystals and has been observed in almost all the devices with room-temperature $\mu_{4p} > 10$ cm^2 V^{-1} s^{-1}. Interestingly, all three devices shown in Figure 2d exhibit band-like transport behavior until $T \leq 100$ K. In other words, the critical transition temperature (T^*) from the intrinsic band-like regime to the shallow-trap-dominated regime can be as low as 100 K. According to Morpurgo and co-workers, a lower T^* means that a smaller degree of static disorder is present in the air-gap transistor.[33] For organic single crystal FETs, such a low T^* has only been reported in high-quality rubrene and deuterated-rubrene (^{2}H-rubrene) single crystals.[34] Based on these results, it is reasonable to say that ^{13}C-rubrene single crystals have essentially the same T-dependent transport as native rubrene.

To further elucidate the intrinsic transport behavior, we carried out Hall measurements on a ^{13}C-rubrene single crystal FET, which displayed band-like transport down to 100 K. **Figure 3**a shows the Hall resistance (defined as $R_{xy} = V_{xy}/I_d$) as a function of magnetic field (B) between 5 T and −5 T at different temperatures with a scan rate of 0.01 T s^{-1}. The gate voltage and source current were fixed at −40 V and 10 nA, respectively. A clear Hall signal with a positive slope can be observed, which is consistent with the p-type conduction in ^{13}C-rubrene FETs. The noise level increases very rapidly upon cooling, so any Hall measurement at $T < 180$ K is prevented, which has been reported earlier in rubrene air-gap transistors.[9] The slope of R_{xy}–B, which is the Hall coefficient $R_H = 1/ep_{Hall}$, increases with decreasing temperature, indicating smaller charge density at lower temperature. We can extract the Hall mobility (μ_{Hall}) from the equations below

$$\mu_{Hall} = \frac{\sigma}{ep_{Hall}} = \frac{R_{xy}}{BR_{xx}}\frac{\Delta L}{W} \quad (4)$$

where σ is the channel conductivity and R_{xx} is defined as $R_{xx} = \Delta V/I_d$. As shown in Figure 3b, both μ_{Hall} and μ_{FET} increase upon cooling and their trends are similar, implying that our device is still in the band-like regime even at 180 K. The Hall measurement confirms that the intrinsic, band-like hole transport has been achieved in ^{13}C-rubrene single crystals.

To compare FET mobilities for ^{13}C-rubrene and native rubrene, we fabricated 74 ^{13}C-rubrene single crystal FETs in order to get a reasonable distribution of field-effect mobility. In addition, another 74 native rubrene single crystal FETs were

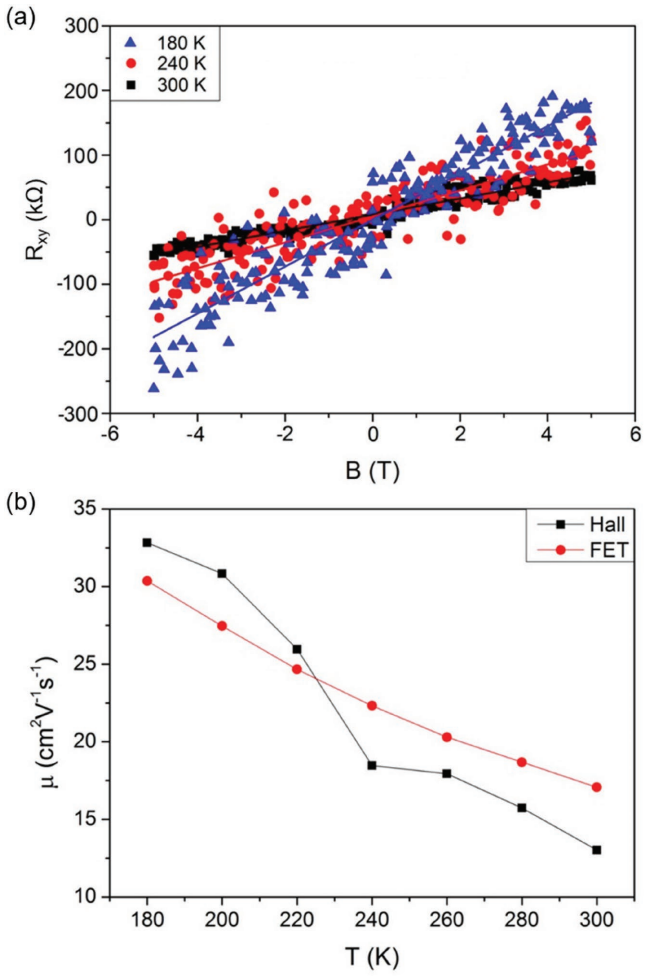

Figure 3. a) Temperature dependence of Hall resistance for a ^{13}C-rubrene air-gap transistor. Measurements were taken at $I_d = 10$ nA and $V_g = -40$ V. This device has dimensions of $\Delta L = 350$ μm and $W = 220$ μm. b) Temperature dependence of the FET and Hall mobility for this device. Band-like transport persists over the whole temperature range ($T > 180$ K) in this device.

fabricated and tested under the same conditions. We find that the mean values for mobility are 12.6 ± 2.2 cm^2 V^{-1} s^{-1} and 14.6 ± 2.4 cm^2 V^{-1} s^{-1}, respectively, for ^{13}C-rubrene and native rubrene, where the uncertainty interval represents 1 standard deviation. However, as many measurements were made, the *t*-test can be employed to find the confidence intervals on the mean values of the mobility, which are the confidence levels of finding the true values in such intervals. Based on the full statistics of mobility in **Figure 4**a, our calculations reveal that even the 99% confidence intervals have no overlap (see the Supporting Information for detailed calculation). The 99% confidence interval on the mean value of mobility for ^{13}C-rubrene single crystal FETs is found to be 12.6 ± 0.7 cm^2 V^{-1} s^{-1}, while that for native rubrene is 14.6 ± 0.7 cm^2 V^{-1} s^{-1}. That is, statistically speaking, the mean values of mobility for native rubrene and ^{13}C-rubrene are truly different and based on the mean values, the isotope effect is –13%. We conclude that we have observed a negative isotope effect on charge transport in rubrene single crystals upon complete ^{13}C-substitution.

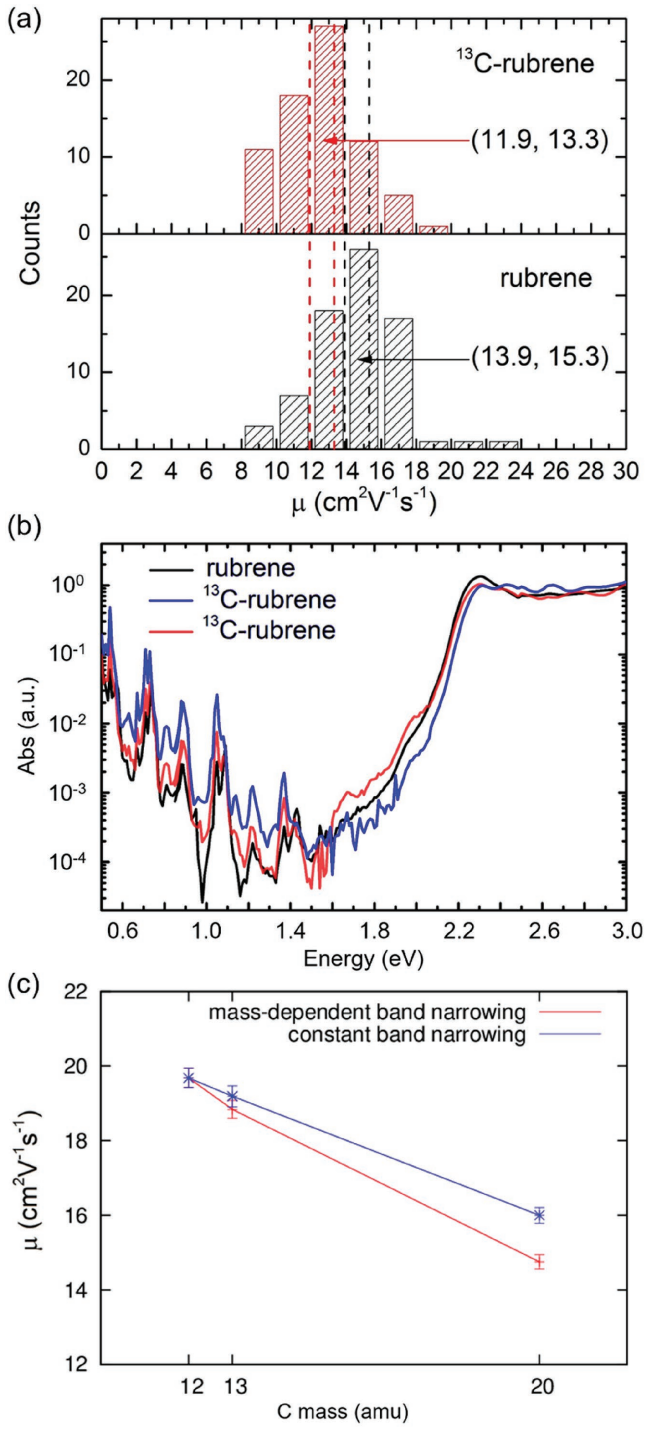

Figure 4. a) Histograms of the room temperature mobility for rubrene and ^{13}C-rubrene. The regions between the dashed lines represent the 99% confidence intervals on the mean values and they have no overlap. b) Photothermal deflection spectroscopy of a native rubrene and two ^{13}C-rubrene crystals. c) Carbon mass dependence of the calculated mobility of rubrene under two different assumptions: mass-dependent band narrowing (red) and constant band narrowing (blue).

It is unlikely that the negative isotope effect is due to extrinsic factors such as impurities or structural defects because the ^{13}C-rubrene crystals exhibit beautiful transport properties as

shown above and are grown under the same conditions after extensive efforts have been made to clean the ^{13}C-rubrene starting material. The purity and structural perfection was confirmed by photothermal deflection spectroscopy, which is a highly sensitive absorption technique that measures the density of optically active sub-bandgap states in organic semiconductors.[35,36] In Figure 4b, it is obvious that both ^{13}C-rubrene and native rubrene have clean bandgaps. Spectra of two different ^{13}C-rubrene crystals are shown here in order to demonstrate that the measurements are reproducible. Moreover, the Urbach energy (E_u), which is determined from an exponential fitting of the absorption band edge across 4 decades of signal, can be used to characterize the atomic disorder in each crystal. Figure 4b reveals that ^{13}C-rubrene and native rubrene have a similar Urbach energy (≈40 meV), which means their degrees of disorder (including both static and dynamic disorder) are comparable. It is thus reasonable to conclude that the origin of the negative isotope effect is the redshift of vibrational frequencies after ^{13}C-substitution as predicted by DDM.

To gain further insight, we carried out simulations based on a numerical model of dynamic disorder introduced by Troisi and Orlandi.[16] In earlier work it was predicted from this numerical model that increasing the molecular mass will cause a decrease in mobility.[16] However, this model did not include the effect of high-frequency modes. It has been reported that the effect of charge coupling to high frequency vibrations is to reduce the transfer integrals between neighboring molecules, which is known as band narrowing.[37,38] This effect effectively decreases l_{loc} and is distinct from the role of low frequency intermolecular modes, which impact μ through ω. Band narrowing is mass-dependent and from Holstein small polaron theory we find that the bandwidth (transfer integral) of ^{13}C-rubrene is 3.5% narrower (this is an upper limit) due to the increased mass (see the Supporting Information). Adding mass-dependent band narrowing to the dynamic disorder scenario, we computed the mobility at 300 K using rubrene parameters taken from a previous publication.[39] The computed mobility decreases from 19.7 to 18.8 cm^2 V^{-1} s^{-1} in going from ^{12}C- to ^{13}C-rubrene, i.e., by 4.5%. If the band narrowing effect is neglected, the mobility reduction is 2.5%. Thus, the simulations confirm a significant negative isotope effect, although the calculated change is smaller than the experimental value. We also calculated the mobility of a hypothetical rubrene where the atomic mass of C is 20 amu to see the isotope effect more clearly (Figure 4c). Indeed, heavier C atoms produce a more pronounced negative isotope effect. The qualitative agreement between experiment and theory broadly supports the dynamic disorder picture of transport in rubrene, but the quantitative discrepancy between the measured and simulated isotope effect suggests opportunities for further investigations. One possible explanation for the difference could be the existence of a sizable feedback between the reduced vibrational frequencies and the presence of unavoidable sources of extrinsic disorder, signaled here by the observed downturn of the mobility at temperatures below ≈100 K. Reduced vibrational frequencies do lead to a reduced hole mobility, but it can also be expected that the resulting slower carriers become more prone to scattering and trapping by impurities and defects, an effect that should further reduce the overall mobility. This hypothesis was confirmed by preliminary calculations in the presence of site disorder, showing that the effect of isotope substitution is enhanced by a factor of two to three (see the Supporting Information).

In summary, we have successfully synthesized ^{13}C-substituted rubrene and systematically investigated the structural and electrical properties of vapor-grown ^{13}C-rubrene single crystals. ^{13}C-rubrene single crystals maintain the intrinsic transport behavior of native rubrene, including hysteresis-free output and transfer characteristics, an average hole mobility over 10 cm^2 V^{-1} s^{-1} at room temperature, and the clear signature of band-like transport persisting to very low temperature ($T \leq 100$ K), with a maximum mobility of ≈45 cm^2 V^{-1} s^{-1} at ≈100 K. The excellent performance of ^{13}C-rubrene single crystal FETs is further confirmed by the observation of the Hall effect in the conducting channel of a ^{13}C-rubrene air-gap transistor, which provides characteristic evidence of the diffusive delocalization of charge carriers over a few molecules. Importantly, we have observed a significant negative isotope effect on charge transport in rubrene single crystals after ^{13}C-substitution, which originates from the decreased vibrational frequencies of ^{13}C-rubrene and supports the physical picture of transport under the influence of dynamic disorder. In a general sense, we believe that ^{13}C isotopic substitution opens new opportunities to understand transport phenomena in organic single crystals.

Supporting Information

Supporting Information is available from the Wiley Online Library or from the author.

Acknowledgements

The work at Minnesota was primarily supported by the National Science Foundation through the University of Minnesota MRSEC under Award Number DMR-1420013. Parts of this work were carried out in the Characterization Facility, University of Minnesota, which receives partial support from NSF through the MRSEC program. D.A.H. was supported in part by an award from The Paul and Daisy Soros Fellowship for New Americans and NSF-GFRP. A.T. acknowledges the support of ERC (Grant No. 615834).

Received: January 13, 2017
Revised: February 15, 2017
Published online: March 15, 2017

[1] R. W. I. de Boer, M. E. Gershenson, A. F. Morpurgo, V. Podzorov, *Phys. Status Solidi* **2004**, *201*, 1302.
[2] M. E. Gershenson, V. Podzorov, A. F. Morpurgo, *Rev. Mod. Phys.* **2006**, *78*, 973.
[3] T. Hasegawa, J. Takeya, *Sci. Technol. Adv. Mater.* **2009**, *10*, 24314.
[4] V. Podzorov, *MRS Bull.* **2013**, *38*, 15.
[5] E. Menard, V. Podzorov, S. H. Hur, A. Gaur, M. E. Gershenson, J. A. Rogers, *Adv. Mater.* **2004**, *16*, 2097.
[6] V. Podzorov, E. Menard, A. Borissov, V. Kiryukhin, J. A. Rogers, M. E. Gershenson, *Phys. Rev. Lett.* **2004**, *93*, 1.
[7] V. C. Sundar, J. Zaumseil, V. Podzorov, E. Menard, R. L. Willett, T. Someya, M. E. Gershenson, J. A. Rogers, *Science* **2004**, *303*, 1644.
[8] C. Reese, Z. Bao, *Adv. Mater.* **2007**, *19*, 4535.

[9] V. Podzorov, E. Menard, J. A. Rogers, M. E. Gershenson, *Phys. Rev. Lett.* **2005**, *95*, 226601.
[10] J. Takeya, K. Tsukagoshi, Y. Aoyagi, T. Takenobu, Y. Iwasa, *Jpn. J. Appl. Phys., Part 2* **2005**, *44*, 1393.
[11] S. Machida, Y. Nakayama, S. Duhm, Q. Xin, A. Funakoshi, N. Ogawa, S. Kera, N. Ueno, H. Ishii, *Phys. Rev. Lett.* **2010**, *104*, 156401.
[12] V. Coropceanu, J. Cornil, D. A. da Silva Filho, Y. Olivier, R. Silbey, J.-L. Bredas, *Chem. Rev.* **2007**, *107*, 926.
[13] S. Fratini, D. Mayou, S. Ciuchi, *Adv. Funct. Mater.* **2016**, *26*, 2292.
[14] A. S. Eggeman, S. Illig, A. Troisi, H. Sirringhaus, P. A. Midgley, *Nat. Mater.* **2013**, *12*, 1045.
[15] D. A. da Silva Filho, E.-G. Kim, J.-L. Bredas, *Adv. Mater.* **2005**, *17*, 1072.
[16] A. Troisi, G. Orlandi, *Phys. Rev. Lett.* **2006**, *96*, 86601.
[17] A. Troisi, *J. Chem. Phys.* **2011**, *134*, 1.
[18] M. Balkanski, R. F. Wallis, *Semiconductor Physics and Applications*, Oxford University Press, New York, USA, **2000**.
[19] Y. Jiang, H. Geng, W. Shi, Q. Peng, X. Zheng, Z. Shuai, *J. Phys. Chem. Lett.* **2014**, *5*, 2267.
[20] R. W. Munn, W. Siebrand, *J. Chem. Phys.* **1970**, *52*, 6391.
[21] R. W. Munn, J. R. Nicholson, W. Siebrand, D. F. Williams, *J. Chem. Phys.* **1970**, *52*, 6442.
[22] D. L. Morel, A. M. Hermann, *Phys. Lett.* **1971**, *36*, 101.
[23] W. Mey, T. J. Sonnonstine, D. L. Morel, A. M. Hermann, *J. Chem. Phys.* **1973**, *58*, 2542.
[24] L. B. Schein, A. R. McGhie, *Phys. Rev. B* **1979**, *20*, 1631.
[25] L. B. Schein, W. Warta, A. McGhie, N. Karl, *Chem. Phys. Lett.* **1980**, *75*, 267.
[26] L. B. Schein, W. Warta, A. R. McGhie, N. Karl, *Chem. Phys. Lett.* **1983**, *100*, 34.
[27] Y. Jiang, Q. Peng, H. Geng, H. Ma, Z. Shuai, *Phys. Chem. Chem. Phys.* **2015**, *17*, 3273.
[28] C. Kloc, P. G. Simpkins, T. Siegrist, R. A. Laudise, *J. Cryst. Growth* **1997**, *182*, 416.
[29] O. D. Jurchescu, A. Meetsma, T. T. M. Palstra, *Acta Crystallogr., Sect. B: Struct. Sci.* **2006**, *62*, 330.
[30] I. N. Hulea, S. Fratini, H. Xie, C. L. Mulder, N. N. Iossad, G. Rastelli, S. Ciuchi, A. F. Morpurgo, *Nat. Mater.* **2006**, *5*, 982.
[31] W. Xie, P. L. Prabhumirashi, Y. Nakayama, K. A. McGarry, M. L. Geier, Y. Uragami, K. Mase, C. J. Douglas, H. Ishii, M. C. Hersam, C. D. Frisbie, *ACS Nano* **2013**, *7*, 10245.
[32] P. V. Pesavento, R. J. Chesterfield, C. R. Newman, C. D. Frisble, *J. Appl. Phys.* **2004**, *96*, 7312.
[33] H. Xie, H. Alves, A. F. Morpurgo, *Phys. Rev. B: Condens. Matter Mater. Phys.* **2009**, *80*, 1.
[34] W. Xie, K. A. McGarry, F. Liu, Y. Wu, P. P. Ruden, C. J. Douglas, C. D. Frisbie, *J. Phys. Chem. C* **2013**, *117*, 11522.
[35] E. Buchaca-Domingo, K. Vandewal, Z. Fei, S. E. Watkins, F. H. Scholes, J. H. Bannock, J. C. De Mello, L. J. Richter, D. M. DeLongchamp, A. Amassian, M. Heeney, A. Salleo, N. Stingelin, *J. Am. Chem. Soc.* **2015**, *137*, 5256.
[36] A. J. Kronemeijer, V. Pecunia, D. Venkateshvaran, M. Nikolka, A. Sadhanala, J. Moriarty, M. Szumilo, H. Sirringhaus, *Adv. Mater.* **2014**, *26*, 728.
[37] K. Hannewald, P. A. Bobbert, *Appl. Phys. Lett.* **2004**, *85*, 1535.
[38] T. Holstein, *Ann. Phys. (N.Y.)* **1959**, *8*, 343.
[39] A. Troisi, *Adv. Mater.* **2007**, *19*, 2000.

